ORIGINAL RESEARCH

Microwave-assisted solvothermal in-situ synthesis of CdS nanoparticles on bacterial cellulose matrix for photocatalytic application

Xin Qian · Yongjian Xu · Xiaopeng Yue · Cai Wang · Min Liu · Chao Duan · Yang Xu · Chao Zhu · Lei Dai

Abstract Bacterial cellulose (BC) is a unique nanofibrous biomaterial, and crystalline cadmium sulphide (CdS) is regarded as one of the most attractive visible light-driven photocatalysts. In this study, a BC@CdS nanocomposite for photocatalytic degradation of organic dye methylene blue (MB) was prepared with a facile and highly efficient strategy. The nanocomposite was prepared through a designed "anchoring-reacting-forming" pathway. SEM images showed that the BC-alcogel was the best matrix for nano-fabrication on which nanosized CdS particles were homogeneously distributed (approximately 100 nm). The results from FT-IR, XRD and XPS revealed that the CdS nanoparticles, mainly cubic and hexagonal crystallite, are attached to the BC fibers via coordination effect. The BC-supported adsorbent photocatalytic material was easy to be recycled and followed a new "adsorption–accumulation–degradation" mechanism of photocatalytic degradation. The results showed BC matrix had a strong adsorption effect on MB molecules, which improved local concentration of MB and promoted the rate of photocatalytic reaction. This novel adsorbent photocatalytic nanocomposite material (contained 12.4% CdS, about 0.91 mg for degradation experiment) possessed highly efficient photocatalytic activity with 77.39% removal of MB after 180 min visible light irradiation (the degradation rate was 28.3% mg^{-1} h^{-1}), and exhibited satisfactory cyclic utilization with slight attenuation. Therefore, BC@CdS nanocomposite is a novel promising candidate as adsorbent photocatalysts with visible light response.

X. Qian (✉) · Y. Xu (✉) · X. Yue · C. Wang · M. Liu · C. Duan · Y. Xu · C. Zhu · L. Dai
Shaanxi University of Science & Technology, Xi'an 710021, Shaanxi, China
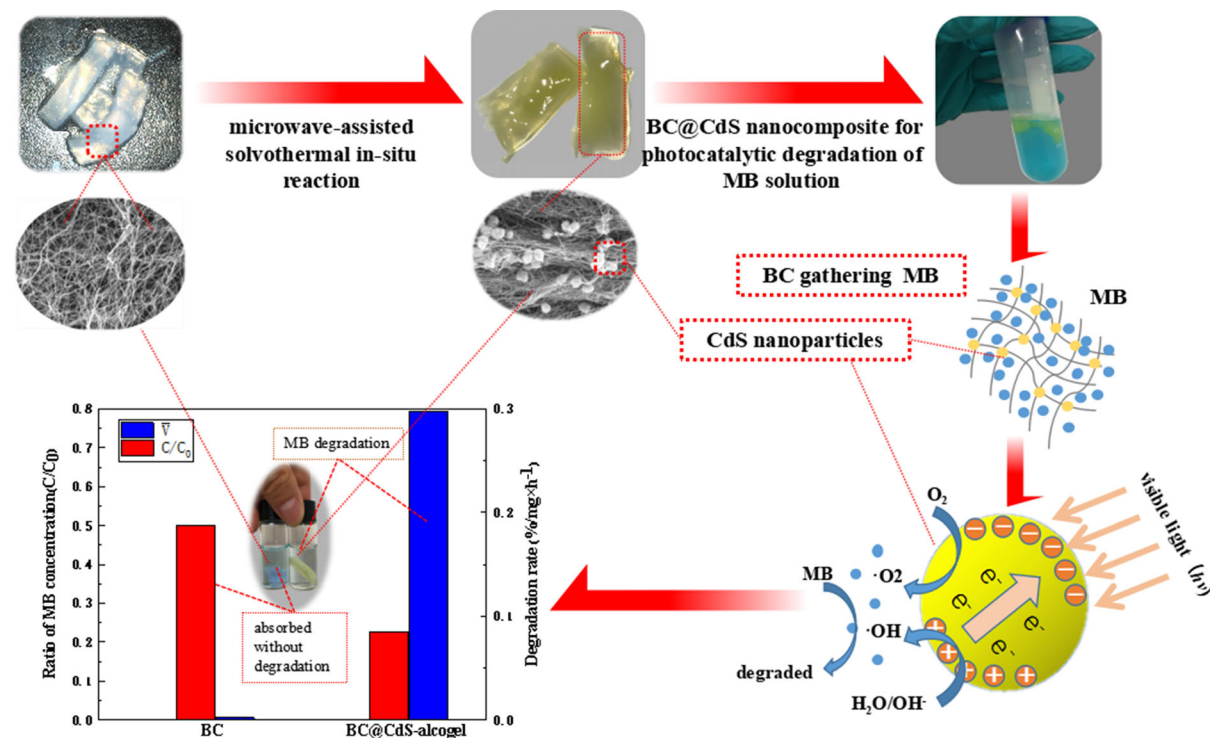e-mail: qianxin@sust.edu.cn

Y. Xu
e-mail: xuyongjian@sust.edu.cn

X. Qian · Y. Xu
Shaanxi Provincial Key Laboratory of Papermaking Technology and Specialty Paper Development (Shaanxi University of Science & Technology), Xi'an, China

X. Qian
National Demonstration Center for Experimental Light Chemistry Engineering Education (Shaanxi University of Science & Technology), Xi'an, China

Y. Xu · X. Yue · C. Duan · L. Dai
Key Laboratory of Paper Based Functional Materials (Shaanxi University of Science & Technology), Xi'an, China

Graphic abstract

Introduction

Under the advocacy of green chemistry principles, biobased materials are increasingly employed in synthetic and catalytic fields. In addition, the design of chemical reaction must take into account two important aspects: enhancing the efficiency of single reaction to reduce energy consumption, as well as fabricating new green materials to meet the environmentally-friendly needs (Jung et al. 2015).

Photocatalytic degradation of pollutants is an efficient, attractive, and clean technology for environmental pollution abatement in both aqueous media and gas phase. There has been extensive research done in this area since the discovery of water splitting on semiconductor catalysts in 1972 (Fujishima and Honda 1972; Yang et al. 2013). As a typical n-type semiconductor nanocrystal of group II–VI, crystalline CdS is regarded as one of the most attractive visible light-driven photocatalysts due to its relatively narrow band gap (Eg = 2.42 eV, corresponding well to the spectrum of sunlight) (Dukovic et al. 2010; Hernández-Gordillo et al. 2013; Meng et al. 2017; Zhu et al. 2015). The relevant researches demonstrate that the morphology of CdS has a significant influence on the optical band gap which determines the performance of photocatalytic degradation (Bera et al. 2015; Liu et al. 2017). More recently, organic–inorganic hybrid materials with excellent properties have emerged as a new type of composite and attracted interests from many researchers around the world. For this reason, various CdS based materials with different morphologies and nanostructures (e.g., nanosheets, nanocrystals, nanowires and nanoparticles) were fabricated using inorganic or organic substrates as templates, creating potential applications in many fields including but not limited to photocatalysis (Cao et al. 2010; Chen et al. 2018; Liang et al. 2004; Shi et al. 2004; Zhou et al. 2006). For facilitating the reuse of the photocatalyst, a few studies on immobilization of CdS on inorganic or organic substrates (such as PVP, PEI-PEG, nafion membrane, ZnO layer) have been carried out (Qi et al.

2000; Venkatareddy et al. 2018; Wang et al. 2005, 2018; Zeng et al. 2002).

Under the enlightenment of bio-inspired fabrication (Maghsoudi-Ganjeh et al. 2019), many bio-based materials (e.g., cotton, silk, chitosan) were used as bio-templates for nano-fabrication (Drachuk et al. 2017; Lai et al. 2009; Li et al. 2016). Among these various bio-based materials, BC produced by fermentation of *Acetobacter xylinum* is a nanofibrous biomaterial and has been modified to fabricate nanocomposite materials for many applications including plant biomimicking, as well as biomedical, electrically conductive, optical, luminescent, proton conductive, antimicrobial, thermo-responsive applications (Qiu and Netravali 2014; Wang et al. 2019). BC has also been widely used as a matrix to fabricate nanocomposite for catalytic application, because it has unique properties such as high Young's modulus (138 GPa), good tensile strength (> 2 GPa), high purity (free of lignin and hemicellulose), good water holding capacity, high crystallinity and excellent biocompatibility (Kashcheyeva et al. 2019). For example, Zhang et al. fabricated BC@TiO_2 nanocomposite by immersing BC blocks into preceramic polymer solution of titanium source for photocatalytic degradation of Rhodamine B (Zhang et al. 2018). In addition, Wei et al. synthesized $CoSe_2$ nanoparticles growing on carbon nanofibers (derived from BC fibers) as an efficient electrocatalyst for hydrogen evolution reaction (Wei et al. 2018). The unique porous 3D nanofibrous structure of BC matrix provided very high specific surface area containing plenty of active hydroxyl groups, which significantly enhanced the metal ion adsorption (Chaiyasat et al. 2019; Chen et al. 2009). Thus, it is feasible for BC to serve as an excellent matrix in the in-situ synthesis of CdS nanoparticles, and the application of BC will simplify the process of nano-fabrication and make the photocatalyst recycling easier. BC@CdS nanocomposite will be an excellent photocatalytic material because it can combine the unique properties of BC with the strong photocatalytic performance of CdS. Due to the existence of BC matrix, it can be expected that the novel adsorbent photocatalytic material will achieve enhanced photocatalytic performance and exhibit better cyclic utilization.

In this study, CdS nanoparticles were synthesized on different BC matrices by a highly efficient microwave-assisted solvothermal in-situ method (quick-heating and reacting, low-energy consumption, Bharti et al. 2018). A possible mechanism was proposed for the growth of CdS nanoparticles on BC and verified by Zeta potential and FT-IR analysis. The morphologies and crystal forms of CdS nanoparticles were also characterized using SEM, XRD and XPS. This study provided a facile, highly efficient wet chemical strategy to synthesize visible light responsive BC@CdS nanocomposite, with its adsorption and photocatalytic performance demonstrated by the degradation of MB. The overall formation mechanism and photocatalytic degradation process of BC@CdS nanocomposite are shown in Fig. 1.

Experimental

Materials and reagents

The fermentative hydrogel-like BC membranes were kindly provided by Tropical Fruits Processing Co. Ltd, Hainan, China. The BC membranes with average thickness of 3 cm, briefly boiled and treated three times with 0.1 M aqueous NaOH at 90 °C for 20 min to remove the bacteria and their residues, were cut into block-shaped pieces. The as-prepared BC membranes were thoroughly washed by deionized water to neutral. Other reagents were all purchased from Kemiou Chemical Reagent Co. Ltd, Tianjin, China, and used without further purification.

The preparation of different BC matrices

Different BC matrices were employed for the synthesis of CdS nanoparticles, including BC-hydrogel, BC-alcogel, and BC-aerogel.

BC-hydrogel The obtained hydrogel-like BC membranes (purified by the method mentioned above in Sect. 2.1) were cut into small blocks for experimental use.

BC-alcogel The BC-hydrogel was subjected to a solvent exchange in absolute ethanol stepwise to obtain BC-alcogel. Firstly, the BC-hydrogel was immersed in the absolute alcohol (50:50, v/v) for 12 h to obtain 50% BC-alcogel. Subsequently, 50% BC-alcogel was transferred to another fresh absolute ethanol bath for 12 h, then the 75% BC-alcogel was obtained. Lastly, the above step was repeated until the
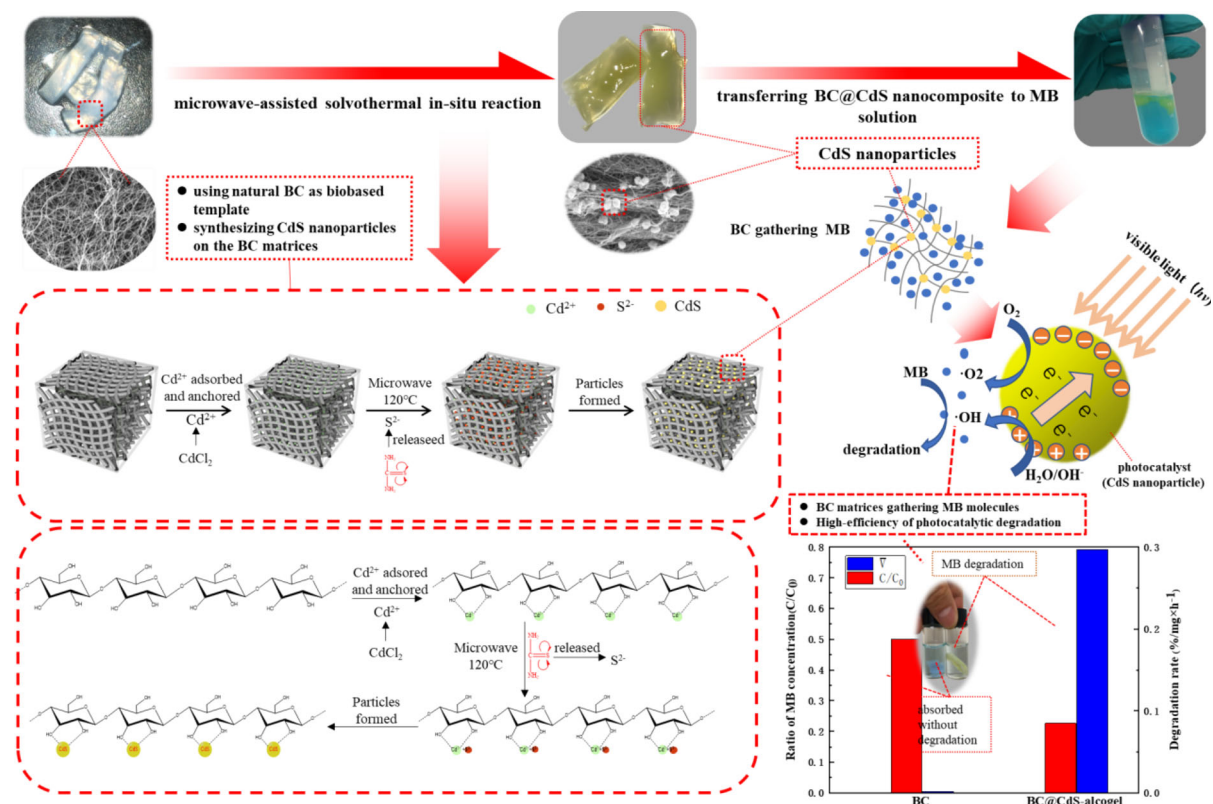
Fig. 1 Schematic representation of the formation mechanism and photocatalytic degradation process of BC@CdS nanocomposite

ethanol content rising up to 99%, and the BC-alcogel was prepared.

BC-aerogel The BC-hydrogel was subjected to freeze drying process to obtain BC-aerogel for experimental use.

Synthesis of BC@CdS nanocomposite

CdS nanoparticles were synthesized on different BC matrices (BC-hydrogel, BC-alcogel and BC-aerogel) using a microwave-assisted solvothermal in-situ method, and each BC block contained almost 7 mg dry BC fibers. Firstly, the squeezed BC-hydrogel, BC-alcogel (0.4 MPa, 5 min, Kumagai Rikii Kogyo Co. Ltd, Japan) and BC-aerogel were immersed into beakers containing 10 ml of 5 mmol/L $CdCl_2$ aqueous alcohol solution (3:2, v/v) with continuous stirring (< 100 rpm) until reaching an adsorption equilibrium. Subsequently, the BC matrices were taken out and rinsed with deionized water several times to remove dissociated Cd^{2+} prior to transferring to another beaker containing 10 mL of 30 mmol/L thiourea

aqueous alcohol solution (3:2, v/v). Thirdly, the matrices with thiourea solution were transferred to microwave synthesis reactor (Monowave 100, Anton Paar, Austria) and irradiated for 3 h at 120 °C after adjusting pH value to 9 with 0.1 mol L^{-1} NaOH aqueous solution. In the process, it was observed that the BC matrices changed to a yellowish color as shown in Fig. 1. Finally, the hybrid nanocomposite was further washed with deionized water and ethanol three times separately and dried overnight by freeze-drying system (alpha 1–4 LD plus, Christ, Germany) for characterization. The mass percentage of CdS was calculated in BC matrix based on the following Eq. 1:

$$w_t\%(CdS) = \frac{W_n - W_0}{W_n} \times 100\% \qquad (1)$$

In Eq. 1, where W_n is the weight of dry BC@CdS nanocomposite, W_0 is the weight of dry BC gels.

Characterization of BC@CdS nanocomposite

The morphology of the BC@CdS nanocomposite was characterized with a Vega-3-SBH (Tescan, Czech) SEM apparatus at 10 kV. Before observation, the surface of the nanocomposite was coated with gold under vacuum. EDS analysis was further performed on this scanning electronic microscopy without gold spraying.

FT-IR spectra of the specimens were collected on a Vertex 70 FT-IR spectrometer (Bruker, Germany) in the range of 4000–400 cm^{-1} with a scan number of 32 times by using the method of KBr pellets.

The surface charge variation was characterized for BC fibers during synthetic process by a MÜTEK SZP-06 Zeta potential system, and the concentration of BC slurry was 0.5% (w/w) for test after homogeneous processing.

XRD pattern of the nanocomposite was obtained on an Advanced D8 XRD apparatus (Bruker, Germany) equipped with a Cu Kα radiation (k = 1.54 A°) as an X-ray resource, which operated (40 kV, 30 mA) at a scan rate of 0.1 per second in a 2θ range of 10°–60°. Before testing, the specimens were vacuum-dried at 60 °C for 12 h.

X-ray photoelectron spectroscopy (XPS, Escalab 250Xi, Thermo Fisher, America) measurements were performed on a PHI-5000 X-ray photoelectron spectrometer with an Al Kα excitation source (100.00 eV).

Thermal stability of the BC@CdS nanocomposite obtained was evaluated using thermogravimetric analyses (TGA). The thermograms were obtained using STA 449 F thermal analyzer (Netzsch, Germany) at a temperature range from 30 to 800 °C with a heating rate of 10 °C/min in N_2 flow.

Adsorption performance of BC@CdS nanocomposite

Adsorption capacity

The adsorption measurement was performed with a Lambda 25 UV–Vis spectrophotometer (PerkinElmer, America) at λ_{max} = 664 nm for the color intensity of MB. The concentration of MB was calculated on the basis of the standard curve for MB solution (S-Fig. 1).

The calculations of the adsorption capacity (q) were performed by the following Eq. 2:

$$q = \frac{(C_0 - C_e)V}{m} \tag{2}$$

where m is the weight of dry BC, C_0 is the initial concentration of the MB solution, Ce is the equilibrium concentration of MB, and V is the volume of the MB solution.

Adsorption kinetics

BC@CdS nanocomposite (1.1 g) was immersed in 20 mL MB solution of 20 mg L^{-1} at room temperature until the adsorption equilibrium. At regular time intervals, the absorbance value of residual solution was measured and the adsorption capacity was calculated. The adsorption kinetics were calculated and determined in accordance with pseudo-first-order (Eq. 3) and pseudo-second-order kinetic models (Eq. 4) as described below (Duan et al. 2019).

$$\ln(q_e - q_t) = \ln(q_e) - K_1 t \tag{3}$$

$$\frac{t}{q_t} = \frac{1}{K_2 q_e^2} + \frac{t}{q_e} \tag{4}$$

where K_1 is the pseudo-first-order rate constant (mg·g^{-1}·min^{-1}), K_2 is the pseudo-second-order rate constant (mg·g^{-1}·min^{-1}), q_e (mg·g^{-1}) is the sorption capacity at equilibrium, q_t (mg·g^{-1}) is the sorption at the time of t.

Effect of pH value

Initial pH value of MB solution (20 mg L^{-1}) was adjusted by 0.1 mol L^{-1} HCl or NaOH aqueous solution to change between 1.0 and 13.0 (1.0, 3.0, 5.0, 7.0, 9.0, 11.0,13.0). BC@CdS nanocomposite (1.0 g) was immersed in 20 mL of MB solution at room temperature for equilibrium time.

Adsorption isotherms

BC@CdS nanocomposite (1.1 g) was immersed into 20 mL MB solution with concentrations of 5 mg·L^{-1}, 10 mg·L^{-1}, 15 mg·L^{-1}, 20 mg·L^{-1} and 25 mg·L^{-1} at 293 K for equilibrium time. The same procedures were applied at 303 K and 313 K. The adsorption isotherms were modeled by using the Langmuir and Freundlich isotherm models (Cheng et al. 2016).

Photocatalytic degradation activity of BC@CdS nanocomposite

Photocatalytic degradation tests were performed using MB (a representative organic dye) as a model contaminant under visible light irradiation with a Xe lamp. The degradation performance of the specimens was determined by measuring absorbance value ($\lambda = 664$ nm) of MB aqueous solution on a Lambda 25 UV–Vis spectrophotometer (PerkinElmer, America), the concentration of MB was calculated on the basis of absorbance of the standard curve (adsorbance to concentration, S-Fig. 1) of MB solution.

The experiments were performed following the steps below: BC and BC@CdS were firstly transferred into test tubes containing MB aqueous solution (20 mL, 20 mg/L). Prior to visible light irradiation, the suspensions were magnetically stirred for 30 min in the dark to reach adsorption/desorption equilibrium. Typically, the total concentration of MB was determined from the maximum adsorption ($\lambda = 664$ nm) measurements by UV–Vis spectroscopy. C_t/C_0 (C_t and C_0 are the concentration of MB at time t and 0 h) was used to describe the degree of MB degradation.

Results and discussion

Analysis of the formation process of CdS nanoparticles on BC matrices

According to Fig. 2a, a possible "anchoring-reacting-forming" pathway is proposed to reveal the formation mechanism of the CdS nanoparticles on BC matrix. In the synthetic process, Cadmium cations (Cd^{2+}) were anchored on BC fibers by ion–dipole interaction (Shim et al. 2002) when BC matrix was immersed into $CdCl_2$ solution. After being rinsed sufficiently to remove unanchored Cd^{2+}, the BC matrix with immobilized Cd^{2+} was transferred to thiourea solution, and CdS nanoparticles were formed on BC 3D networks when thiourea released S^{2-} with the effect of microwave. It was clear that the semitransparent BC matrix changed to a bright yellowish color (as shown in Fig. 1).

Figure 2b shows the results of FT-IR spectra for BC, BC/Cd^{2+} and BC@CdS nanocomposite. The results support the assumptive mechanism of the forming process. It can be seen that the peak at 3390 cm^{-1} corresponding to –OH stretching vibration

declines to lower wavenumber (3343 cm^{-1}) after transferring BC into $CdCl_2$ solution and reaching the adsorption equilibrium, and the area of the peak decreases sharply. When CdS nanoparticles form on BC matrices (curve BC@CdS), the peak corresponding to –OH vibration obviously moves to higher wavenumber (3361 cm^{-1}) with the increasing of the peak area (larger than curve BC/Cd^{2+} and smaller than curve BC). This indicates that the hydroxyl groups are the main active sites during the in-situ synthesis process. In the process, the hydroxyl groups of BC form strong coordination effect with CdS nanoparticlesMeanwhile, the peaks around 2976 cm^{-1}, 1651 cm^{-1}, 1049 cm^{-1} corresponding to stretching vibration of C–H, C=O, and C–O–C groups exhibit the same trends with the peak of 3390 cm^{-1}, which reconfirms the coordination effect is the main interaction between BC matrix and CdS nanoparticles.

Secondly, Zeta potential is frequently employed to characterize fibers surface charge, which consists of plentiful surface hydroxyl groups of fibers. Figure 2c shows the Zeta potential variation after adding reagent $CdCl_2$ into BC slurry. Zeta potential of BC fibers rises from − 29.3 mV (containing no Cd^{2+}) to -5.1 mV and finally stabilizes at − 6.3 mV (containing Cd^{2+} with the concentration of 5 mmol/L). This indicates that Cd^{2+} ions are adsorbed by hydroxyl groups and anchored by ion–dipole interaction.

The characterization of BC@CdS nanocomposite

The analyses were carried out for characterization of BC@CdS nanocomposite with SEM, EDS, XRD and XPS. The results are shown in Figs. 3, 4, and 5.

As is shown in Fig. 3a, pure BC matrix exhibits 3D self-supported structure containing porous and interconnected tunnels, which forms in the self-assemble process of bacterial cultivation. Figure 3b–d show SEM images of different BC@CdS nanocomposite. CdS particles on BC-hydrogel (Fig. 3b) agglomerate together and display inhomogeneous sizes because of the impact of bound-water in BC matrix. CdS particles on BC-alcogel (Fig. 3c) exhibit nanoscale sizes (approximately 100 nm) and distribute homogeneously. Besides, CdS particles on BC-aerogel exhibit much wider and bigger size (about 300–700 nm).

To identify the existence of the element Cd and S in BC@CdS nanocomposite, EDS analysis was proceeded. In Fig. 3e, Cd and S can be observed clearly,
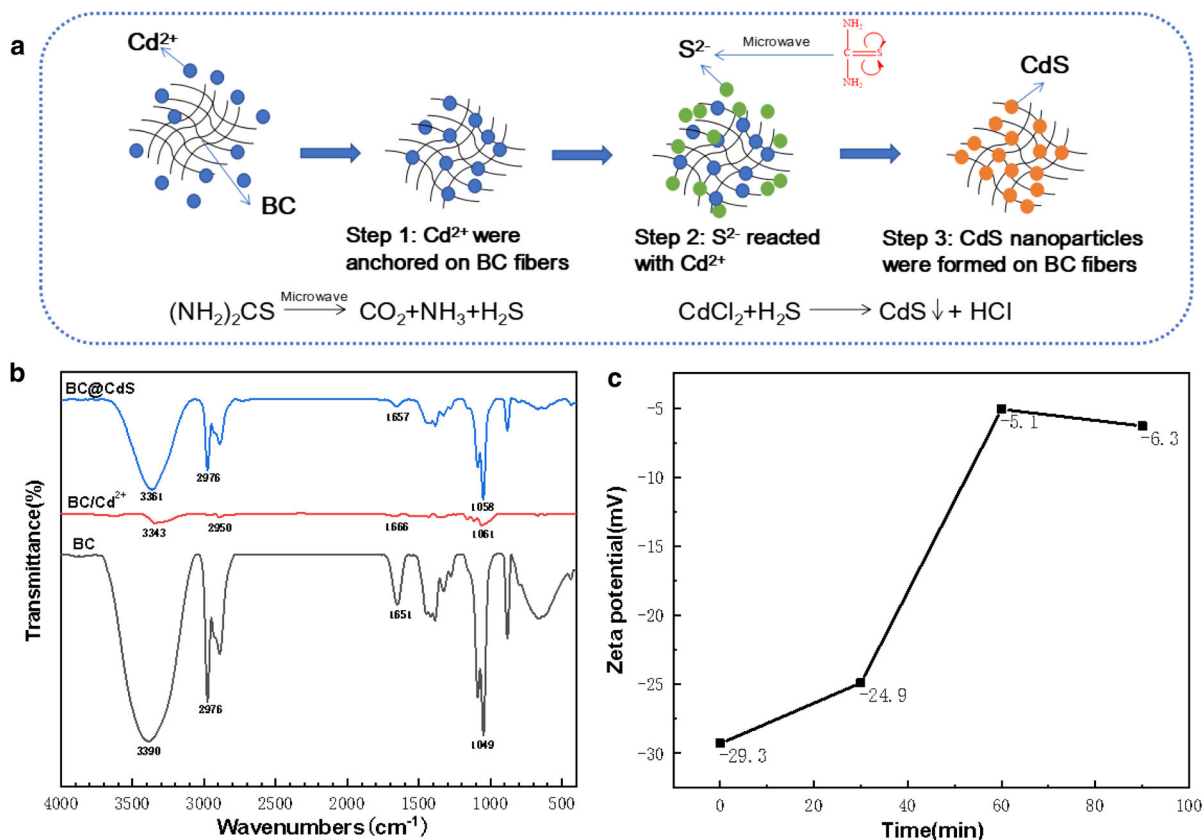
Fig. 2 The analysis of forming process of CdS nanoparticles on BC matrix. **a** Assumptive forming process of CdS nanoparticles; **b** FT-IR spectra of BC, BC/Cd^{2+} and BC@CdS nanocomposite; **c** Zeta potential curve of BC fibers in the process of adsorbing Cd^{2+}

demonstrating that CdS nanoparticles are synthesized on BC matrices by in-situ method. Meanwhile, the loading percentage of CdS on different BC matrices is calculated and shown in Table 1. BC-aerogel is loaded with the most quantity of CdS (13.2% ± 0.3%) while BC-alcogel supports less mass of CdS (12.4% ± 0.3%), and BC-hydrogel bears the minimum weight of CdS (10.5% ± 0.3%).

The reasons for this phenomenon are as follows: the bound-water molecule layer on BC fibers has stronger polarity than ethanol molecules layer, which influences the homogeneity and quantity of adsorption of Cd^{2+} on BC fiber. The stronger polarity causes heterogeneous dispersion of CdS particles and minimizes CdS loading percentage. Meanwhile, the lack of ethanol results in uncontrolled growth of CdS particles on BC-aerogel, leading to much bigger size and increased loading percentage of CdS at the end. It can be concluded that BC-alcogel is the best matrix for synthesis of CdS nanoparticles.

Figure 4 shows three intensive diffraction peaks appearing at 14.6°, 16.9° and 22.8° corresponding to the crystallographic planes of (100), (010) and (110) of BC fibers (French 2014). Due to the presence of electron-rich Cd and sulfur, the peak intensities from the BC are diminished. To check the crystalline phase of CdS on the BC matrix, characteristic peaks from 23° to 60° which contains most of the peaks of CdS are also shown in Fig. 4. BC@CdS-alcogel nanocomposite presents prominent diffraction peaks at 2θ values of 24.8°, 26.5°, 28.2°, 36.6°, 43.7° and 51.8° which is corresponding with the (100), (002), (101), (102), (110), (112) planes of pure CdS standard card (JCPDS Card 41-1049) respectively. All of the diffraction peaks match well with those of the perfect hexagonal wurtzite-structured CdS (Zhou et al. 2019).
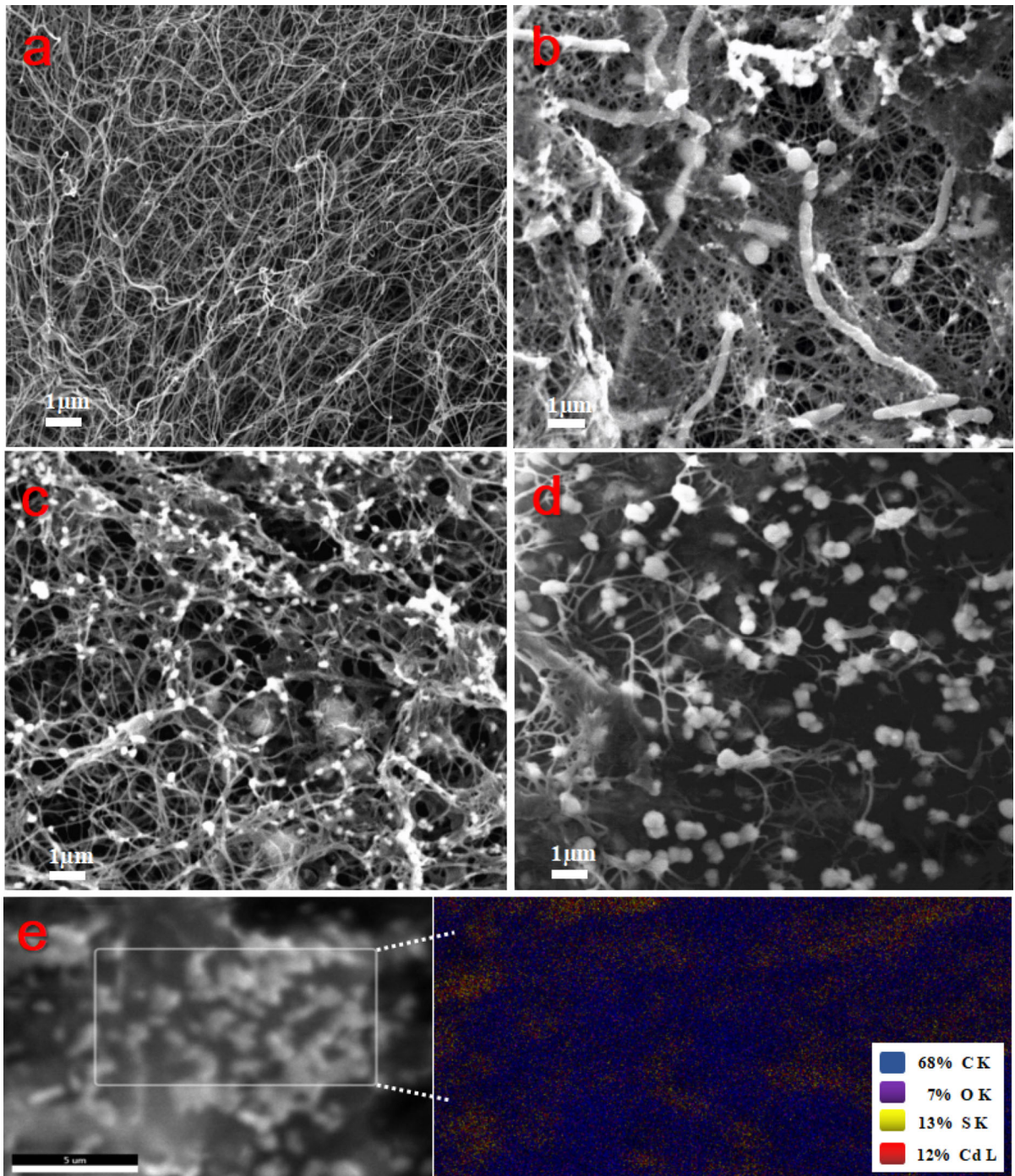
Fig. 3 SEM images of BC (**a**), BC@CdS-hydrogel (**b**), BC@CdS-alcogel (**c**), BC@CdS-aerogel (**d**); EDS analysis of BC@CdS nanocomposite (**e**)

Furthermore, BC@CdS-alcogel nanocomposite has other diffraction peaks at 26.4°, 43.8° and 51.9° corresponding with the (111), (220), (311) planes of pure CdS standard cards (JCPDS 65–2887). This confirms that the cubic structure of CdS has been synthesized on BC fibers (Li et al. 2009). The results

Fig. 4 XRD patterns of BC
and BC@CdS-alcogel
nanocomposite
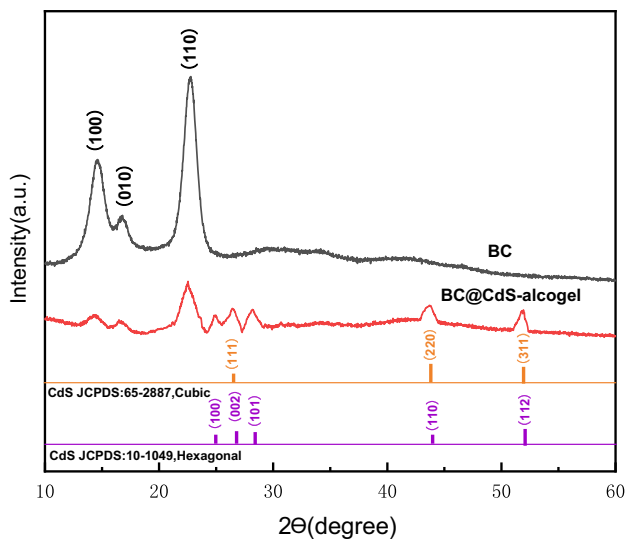
clearly indicate that cubic and hexagonal crystalline phases of CdS nanoparticles coexist in BC-alcogel.

Further evidence was obtained for the high crystal quality by using XPS. As is shown in Fig. 5a and b, the binding energies of both O 1s and C 1s are identified respectively at 532.87 eV and 286.57 eV, which correspond to the glucose chain of BC fibers. From Fig. 5c and d, the binding energies of S 2$p_{3/2}$, Cd 3$d_{3/2}$ and Cd 3$d_{5/2}$ are identified at 161.57 eV, 411.97 eV and 405.27 eV, which are consistent with the reported values in the literature (Xiong et al. 2009; Zhai et al. 2009). These results further confirm that the nanoparticles are pure CdS, which has been proven in the XRD results. According to XPS results, the percentage of Cd atom is 0.85%, the percentage of S atom is 0.61%, and the atomic ratio of Cd to S is calculated to be 1.37, indicating that almost Cd^{2+} ions are transformed to CdS nanoparticles.

Thermostability of BC@CdS nanocomposite

Thermostability is an important property of nanocomposite for future applications. Figure 6a and b shows TGA and DTG curves of BC and BC@CdS-alcogel nanocomposite. The TGA curves (Fig. 6a) of these two specimens exhibit two stages of weight loss in the temperature range from 30 to 780 °C. The weight loss below 140 °C is attributed to water evaporation. In the temperature range from 220 to 370 °C, a huge weight loss can be observed due to the degradation of cellulose. The decomposition temperature of BC is

about 330 °C, whereas the decomposition temperature of BC@CdS-alcogel nanocomposite shifts to a higher temperature due to insertion of CdS. According to DTG curves (Fig. 6b), the BC@CdS-alcogel nanocomposite requires much higher temperature than natural BC when reaching the highest degradation rate. This indicates that CdS nanoparticles are efficiently inserted in BC-alcogel.

Adsorption performance of BC@CdS nanocomposite

Figure 7a shows a real process and a possible mechanism of photocatalytic degradation of BC@CdS nanocomposite. A new photocatalytic degradation model "adsorption–accumulation–degradation" is proposed. As is shown in Fig. 7a, pure BC just possesses ability of adsorption for MB molecules without degradation after 180 min visible light irradiation. On the contrast, BC@CdS nanocomposite exhibits clear photocatalytic degradation effect on MB. The comparison on maximum equilibrium sorption capacity of different adsorbents for MB is shown in Table 2.

The adsorption performance of BC@CdS nanocomposite for MB was also investigated. Figure 7b shows the changes of adsorption capacity of BC@CdS nanocomposite for MB over time. It can be seen that the adsorption capacity increases dramatically and quickly reaches adsorption equilibrium within 30 min, which indicates that there is a strong
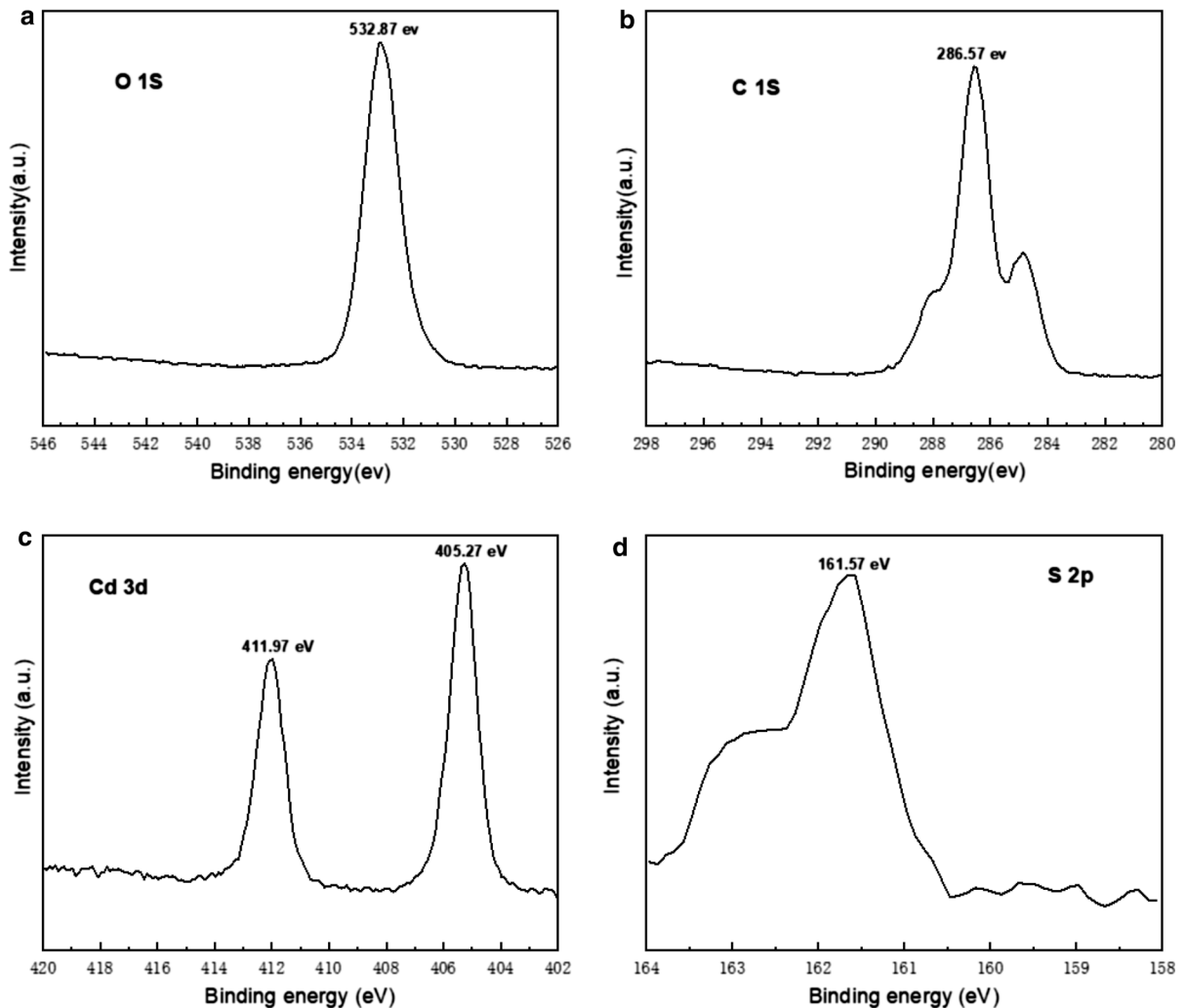
Fig. 5 XPS analysis of BC@CdS-alcogel nanocomposite (**a–d**)

Table 1 The loading percentage of CdS on BC-hydrogel, BC-alcogel and BC-aerogel

Samples	Average mass of dry BC (mg)	Average mass of BC@CdS (mg)	Loading percentage of CdS (%)
BC-hydrogel	7.20	8.04	10.5 ± 0.3
BC-alcogel	7.25	8.28	12.4 ± 0.3
BC-aerogel	6.50	7.49	13.2 ± 0.3

interaction between adsorbent (BC@CdS nanocomposite) and adsorbate (MB).

Figure 7c shows the adsorption kinetic curve of the nanocomposite. The constants of the kinetic process are calculated and shown in Table 3. It is concluded that the linear correlation coefficient ($R^2 = 0.99996$)

simulated by pseudo-second-order kinetics is much better than that ($R^2 = 0.82899$) simulated by pseudo-first-order kinetics. The R^2 of the fitted curves for the two models suggests that the pseudo-second-orders model is more suitable to describe the adsorption kinetic behavior of the BC@CdS nanocomposite for
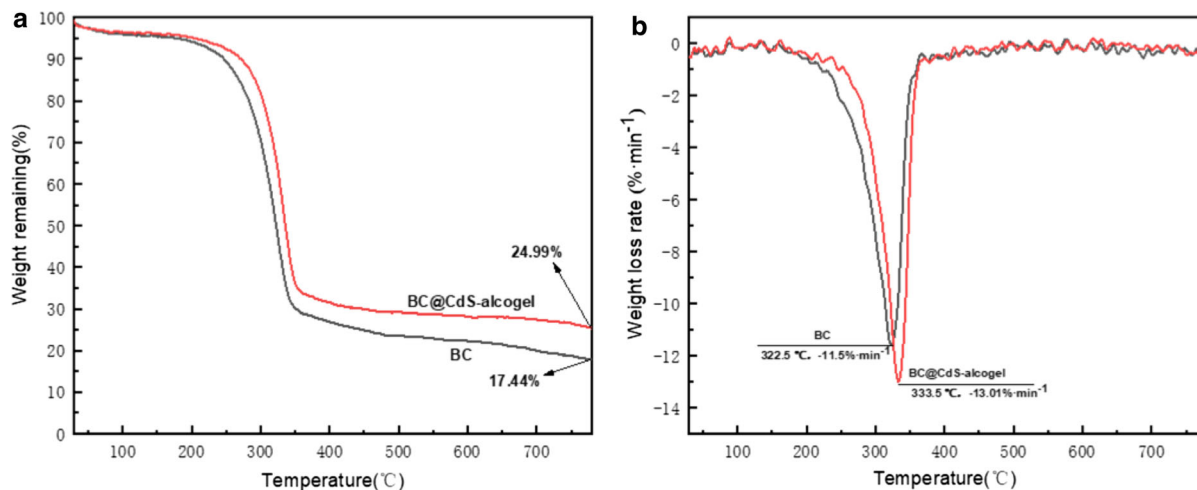
Fig. 6 TG and DTG curves of BC and BC@CdS-alcogel nanocomposite

MB, which demonstrates that the adsorption behavior is controlled by chemical adsorption process (Chen et al. 2019).

Figure 7d shows that the pH value plays a significant role during the adsorption process. With pH value increasing, the adsorption capacity of BC@CdS nanocomposite for MB increases at first and then decreases, the nanocomposite reaches the highest adsorption capacity at neutral pH. The adsorption ability of BC@CdS nanocomposite for MB is attributed to the electrostatic attraction between the negative charges of the adsorbent surface and the positive charge of the MB cation. The negatively charged sorption sites (C–O$^-$), existing on the surface of BC, can adsorb the cationic dyes such as MB. At low pH value, the negatively charged sorption sites are protonated to form C–OH$_2^+$ by H$^+$, which decreases surface negative charge of BC and reduces the adsorption capacity (Auta and Hameed 2014). When the pH value increases, OH$^-$ will influence the positive charge of MB cation, the sorption sites on the surface of BC fibers are harder to attract MB cation. So neutral pH value is beneficial for adsorption of MB.

Adsorption isotherms of BC@CdS nanocomposite for MB at different temperature (293 K, 303 K, 313 K) are presented in Fig. 7e. The adsorption capacity increases with the increase in MB concentration and surrounding temperature. This indicates that higher initial concentration of MB and surrounding temperature is advantageous for adsorption. The

parameters of Langmuir model and Freundlich model are calculated and listed in Table 4. The best fit isotherm model for the system is compared by judging the correlation coefficients and R^2 values. The Langmuir model shows the best fit with the highest R^2 values at all temperatures compared with Freundlich model, suggesting that monolayer coverage of MB adsorbing onto the adsorbate (Liu et al. 2010).

The photocatalytic performance of BC@CdS nanocompsite

The photocatalytic performance of BC@CdS-alcogel nanocomposite was studied. It can be seen in Fig. 8a, BC and BC@CdS-alcogel nanocomposite exhibits high adsorption ability within the first 30 min in darkness. The concentration of MB decreases to 60% because large quantities of MB molecules are adsorbed on BC surface. During the next 180 min, the reaction turns into accumulation and degradation stage, the nanocomposite exhibits highly degradation activity in comparison with pure BC. Finally, BC@CdS-alcogel nanocomposite shows high efficiency with 77.39% MB degradation after 180 min visible light irradiation. The strong adsorption of BC matrix for MB improves local concentration and promotes activity of photocatalytic degradation.

Figure 8b shows the results from the cyclic test of BC@CdS-alcogel nanocomposite for MB. The degradation activity of BC@CdS nanocomposite for MB exhibits a slight attenuation after five circles. This
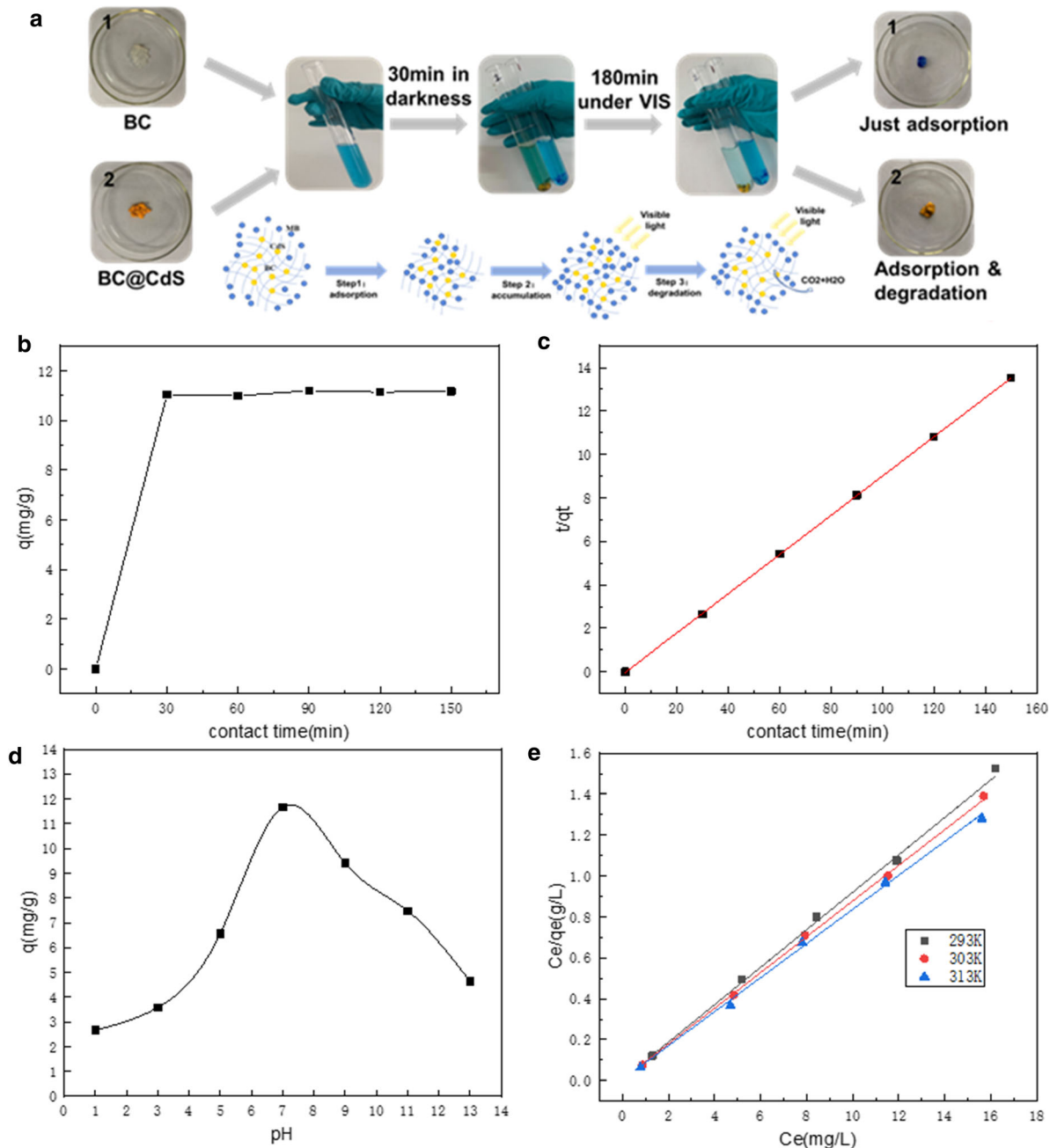
Fig. 7 The possible photocatalytic degradation mechanism of BC@CdS nanocomposite (**a**); the adsorption performance of BC@CdS nanocomposite for MB (**b–e**)

proves that the BC@CdS nanocomposite has good cyclic utilization. Table 5 shows the comparison of photocatalytic activity among BC@CdS-alcogel, BC@TiO2-air-3 and P$_{25}$. The BC@CdS-alcogel also possesses the highest efficiency ($28.3\% \cdot mg^{-1} \ h^{-1}$) of photocatalytic degradation for MB.

Conclusions

Highly efficient photocatalytic CdS nanoparticles were successfully synthesized on BC matrix by a facile microwave-assisted solvothermal in-situ method. A possible forming mechanism of CdS

Table 2 The comparison on maximum equilibrium sorption capacity of different adsorbents for MB

Adsorbents	q_m (mg g^{-1})	References
Cellulose nanocomposite	11.07	Chen et al. (2016)
Cellulose–attapulgite nanocomposite hydrogel	24.3	Chen et al. (2019)
Cross-linked porous starch	9.46	Guo et al. (2013)
Spent rice biomass	8.3	Rehman et al. (2012)
Bacterial cellulose-alcogel	12.68	This work

Table 3 The adsorption kinetic constants of BC@CdS nanocomposite for MB

Pseudo-first order kinetic			Pseudo-second order kinetic		
K_1 (mg g^{-1} min^{-1})	q_e (mg g^{-1})	R^2	K_2 (mg g^{-1} min^{-1})	q_e (mg g^{-1})	R^2
0.0003	1.6498	0.829	0.8251	11.1037	0.999

Table 4 Adsorption isotherms parameters of BC@CdS nanocomposite for MB

Adsorbate	T (K)	Langmuir model			Freundlich model		
		q_m (mg g^{-1})	K_L (L mg^{-1})	R^2	K_F (L mg^{-1})	$1/n$	R^2
BC@CdS nanocomposite	293	10.92	18.9194	0.999	10.6778	0.0068	0.912
	303	11.45	20.0991	0.999	11.2562	0.0045	0.664
	313	12.00	22.1517	0.999	11.8210	0.0041	0.693
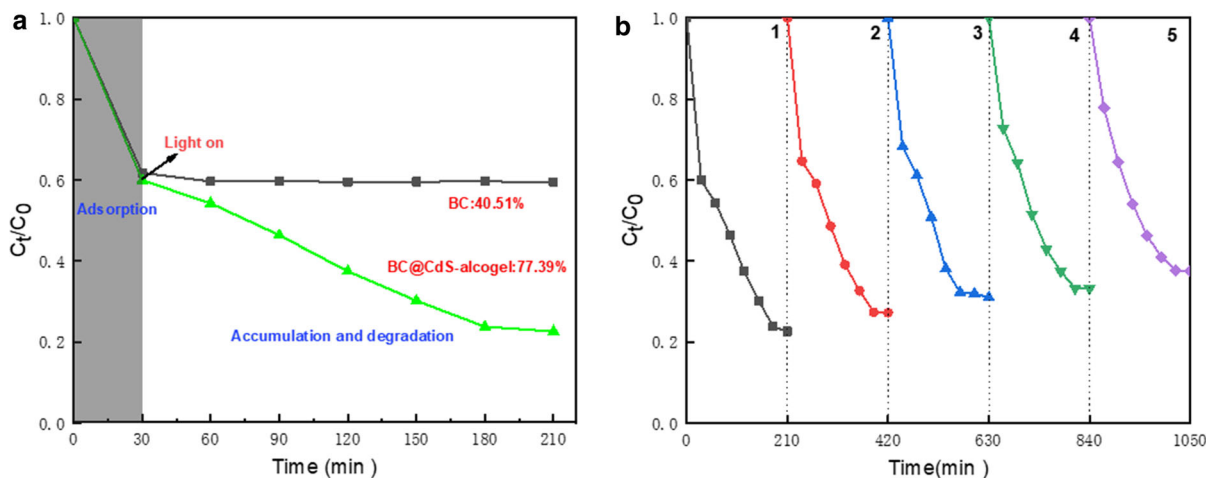
Fig. 8 Photocatalytic degradation performances of BC@CdS-alcogel nanocomposite

nanoparticles on BC matrix was proposed and verified. CdS nanoparticles on different BC matrices exhibited different morphology and different loading percentage. BC-alcogel was found to be the best matrix to prepare CdS nanoparticles, on which cubic and hexagonal CdS nanocrystals (approximately 100 nm) were distributed uniformly. This new kind of organic–inorganic hybrid nanocomposite followed an "adsorption–accumulation–degradation" pathway of photocatalytic degradation. The BC matrix had strong

Table 5 Comparison on photocatalytic activity of different photocatalysts

Photocatalysts	Type of light	Weight (mg)	Loading percentage (%)	Reaction time (min)	Percentage of degradation (%)	Efficiency of degradation (%·mg^{-1}·h^{-1})	References
BC@CdS-alcogel	VIS	7.34	12.4	180	77.39	**28.3**	This work
BC@TiO2-air-3	UV	30	78.7	12	95	**20.1**	Zhang et al. (2018)
P$_{25}$	UV	30	100	12	95	**15.8**	Zhang et al. (2018)

Bold emphsize that the photocatalytic efficiency of BC@CdS-alcogel is higher than the other two samples

adsorption for MB, and the testing results showed that the adsorption kinetics fitted well to the pseudo-second-orders model and adsorption isotherms fitted better to the Langmuir model. Because of the synergistic effect of BC and CdS, this novel adsorbent nanocomposite (contained 12.4% CdS, about 0.91 mg for degradation experiment) was highly efficient for photocatalytic degradation of MB under visible light irradiation (77.39% removal, the degradation rate was 28.3%·mg^{-1}·h^{-1}). It was also convenient for cyclic utilization with slight attenuation.

Compliance with ethical standards

Conflict of interest The authors declare that there are no conflicts of interest.

References

Auta M, Hameed BH (2014) Chitosan-clay composite as highly effective and low-cost adsorbent for batch and fixed-bed adsorption of methylene blue. Chem Eng J 237:352–361. https://doi.org/10.1016/j.cej.2013.09.066

Bera R, Kundu S, Patra A (2015) 2D hybrid nanostructure of reduced graphene oxide–CdS nanosheet for enhanced photocatalysis. ACS Appl Mater Interfaces 7(24):13251–13259. https://doi.org/10.1021/acsami.5b03800

Bharti DB, Bharati AV, Wankhade AV (2018) Synthesis, characterization and optical property investigation of CdS nanoparticles. Luminescence 33(8):1445–1449. https://doi.org/10.1002/bio.3572

Cao BL, Jiang Y, Wang C, Wang WH, Wang LZ, Niu M (2010) Synthesis and lasing properties of highly ordered CdS nanowire arrays. Adv Func Mater 17(9):1501–1506. https://doi.org/10.1002/adfm.200601179

Chaiyasat A, Jearanai S, Christopher LP, Alam MN (2019) Novel superadsorbent materials from bacterial cellulose. Polym Int 68(1):102–109. https://doi.org/10.1002/pi.5701

Chen S, Zou Y, Yan Z, Shen W, Shi S, Zhang X, Wang H (2009) Carboxymethylated-bacterial cellulose for copper and lead ion removal. J Hazard Mater 161(2–3):1355–1359. https://doi.org/10.1016/j.jhazmat.2008.04.098

Chen X, Song XX, Sun Y (2016) Attapulgite nanofiber-cellulose nanocomposite with core-shell structure for dye adsorption. Int J Polym Sci 2016:1–9. https://doi.org/10.1155/2016/2081734

Chen W, Wu W, Yang W, Zhao J, Xiao M, Kong W (2018) CdCl$_2$-assisting heat-treatment: enhanced photoelectrocatalytic hydrogen generation and stability of CdS/ZnO nanoheterojunction arrays. Int J Hydrog Energy 43(21):9969–9977. https://doi.org/10.1016/j.ijhydene.2018.04.045

Chen XY, Chen C, Zhu J (2019) Facile preparation of cellulose attapulgite nanocomposite hydrogel for dye adsorption. Iran Polym J 28(4):347–359. https://doi.org/10.1007/s13726-019-00703-9

Cheng H, Feng Q, Liao C, Liu Y, Wu D, Wang Q (2016) Removal of methylene blue with hemicellulose/clay hybrid hydrogels. Chin J Polym Sci 34(6):709–719. https://doi.org/10.1007/s10118-016-1788-2

Drachuk I, Harbaugh S, Geryak R, Kaplan DL, Tsukruk VV, Kelley-Loughnane N (2017) Immobilization of recombinant *E. coli* cells in a bacterial cellulose-silk composite matrix to preserve biological function. ACS Biomater Sci Eng 3(10):2278–2292. https://doi.org/10.1021/acsbiomaterials.7b00367

Duan C, Meng X, Liu C, Lu W, Liu J, Dai L, Wang W, Zhao W, Xiong C, Ni Y (2019) Carbohydrates-rich corncobs supported metal-organic frameworks as versatile biosorbents for dye removal and microbial inactivation. Carbohydr Polym 222:115042. https://doi.org/10.1016/j.carbpol.2019.115042

Dukovic G, Merkle MG, Nelson JH, Hughes SM, Alivisatos AP (2010) Photodeposition of Pt on colloidal CdS and CdSe/CdS semiconductor nanostructures. Adv Mater 20(22):4306–4311. https://doi.org/10.1002/adma.200800384

Fujishima A, Honda K (1972) Electrochemical photolysis of water at a semiconductor electrode. Nature 238(5358):37–38. https://doi.org/10.1038/238037a0

French AD (2014) Idealized powder diffraction patterns for cellulose polymorphs. Cellulose 21(2):885–896. https://doi.org/10.1007/s10570-013-0030-4

Guo L, Li G, Liu J, Meng Y, Tang Y (2013) Adsorptive decolorization of methylene blue by crosslinked porous starch. Carbohydr Polym 93(2):374–379. https://doi.org/10.1016/j.carbpol.2012.12.019

Hernández-Gordillo A, Romero AG, Tzompantzi F, Gómez R (2013) New nanostructured CdS fibers for the photocatalytic reduction of 4-nitrophenol. Powder Technol 250:97–102. https://doi.org/10.1016/j.powtec.2013.10.008

Jung YH, Chang TH, Zhang H, Yao C, Zheng Q, Yang VW (2015) High-performance green flexible electronics based on biodegradable cellulose nanofibril paper. Nat Commun 6:1–11. https://doi.org/10.1038/ncomms8170

Kashcheyeva EI, Gladysheva EK, Skiba EA, Budaeva VV (2019) A study of properties and enzymatic hydrolysis of bacterial cellulose. Cellulose 26(4):2255–2265. https://doi.org/10.1007/s10570-018-02242-7

Lai S, Chang X, Fu C (2009) Cadmium sulfide quantum dots modified by chitosan as fluorescence probe for copper(II) ion determination. Microchim Acta 165(1–2):39–44. https://doi.org/10.1007/s00604-008-0094-2

Li X, Chen S, Hu W, Shi S, Shen W, Zhang X, Wang H (2009) In situ synthesis of CdS nanoparticles on bacterial cellulose nanofibers. Carbohydr Polym 76(4):509–512. https://doi.org/10.1016/j.carbpol.2008.11.014

Li J, Cao J, Zhang X, Wang S, Zheng Y, Pan J, Li C (2016) Preparation of cotton cellulose nanofibers/ZnO/CdS nanocomposites and its photocatalytic activity. J Mater Sci 27(2):1479–1484. https://doi.org/10.1007/s10854-015-3914-2

Liang H, Angelini TE, Braun PV, Wong GCL (2004) Roles of anionic and cationic template components in biomineralization of CdS nanorods using self-assembled DNA-membrane complexes. J Am Chem Soc 126(43):14157–14165. https://doi.org/10.1021/ja046718m

Liu Y, Zheng YA, Wang AQ (2010) Enhanced adsorption of methylene blue from aqueous solution by chitosan-g-poly (acrylic acid)/vermiculite hydrogel composites. J Environ Sci 22(4):486–493. https://doi.org/10.1016/S1001-0742(09)60134-0

Liu Y, Ma YJ, Liu WW, Shang YY, Zhu AQ, Tan PF (2017) Facet and morphology dependent photocatalytic hydrogen evolution with CdS nanoflowers using a novel mixed solvothermal strategy. J Colloid Interface Sci 513:222–230. https://doi.org/10.1016/j.jcis.2017.11.030

Maghsoudi-Ganjeh M, Lin LQ, Wang XD (2019) Bioinspired design of hybrid composite materials. Int J Smart Nano Mater 10(1):90–105. https://doi.org/10.1080/19475411.2018.1541145

Meng AY, Zhu BC, Zhong B, Zhang LY, Cheng B (2017) Direct Z-scheme TiO$_2$/CdS hierarchical photocatalyst for enhanced photocatalytic H$_2$-production activity. Appl Surf Sci 422:518–527. https://doi.org/10.1016/j.a[sisc/2017.06.028

Qi LM, Cölfen H, Antonietti M (2000) Synthesis and characterization of CdS nanoparticles stabilized by double-hydrophilic block copolymers. Nano Lett 1(2):61–65. https://doi.org/10.1021/nl0055052

Qiu K, Netravali AN (2014) A review of fabrication and applications of bacterial cellulose based nanocomposites. Polym Rev 54(4):598–626. https://doi.org/10.1080/15583724.2014.896018

Rehman MSU, Kim I, Han J-I (2012) Adsorption of methylene blue dye from aqueous solution by sugar extracted spent rice biomass. Carbohydr Polym 90(3):1314–1322. https://doi.org/10.1016/j.carbpol.2012.06.078

Shi J, Qin Y, Wu W, Li X, Guo ZX, Zhu D (2004) In situ synthesis of CdS nanoparticles on multi-walled carbon nanotubes. Carbon 42(2):455–458. https://doi.org/10.1016/j.carbon.2003.11.016

Shim I-W, Noh W-T, Kwon J, Cho JY, Kim K-S, Kang D-H (2002) Preparation of copper nanoparticles in cellulose acetate polymer and the reaction chemistry of copper complexes in the polymer. Bull Korean Chem Soc 23(4):563–566. https://doi.org/10.5012/bkcs.2002.23.4.563

Venkatareddy C, Bandaru N, Reddy IN, Shim J, Yoo K (2018) UV–Visible light driven photocatalytic activities of CdS nanoparticles supported ZnO layers. Mater Sci Eng B 232:68–75. https://doi.org/10.1016/j.mseb.2018.11.004

Wang SM, Liu P, Wang XX, Fu X (2005) Homogeneously distributed CdS nanoparticles in nafion membranes: preparation, characterization, and photocatalytic properties. Langmuir ACS J Surf Colloids 21(25):11969–11973. https://doi.org/10.1021/la051072c

Wang HJ, Cao Y, Wu LL, Wu SS, Raza A, Liu N (2018) ZnS-based dual nano-semiconductors (ZnS/PbS, ZnS/CdS or ZnS/Ag2S,): A green synthesis route and photocatalytic comparison for removing organic dyes. J Environ Chem Eng 6(6):6771–6779. https://doi.org/10.1016/j.jece.2018.10.034

Wang J, Tavakoli J, Tang Y (2019) Bacterial cellulose production, properties and applications with different culture methods: a review. Carbohyd Polym 219:63–76. https://doi.org/10.1016/j.carbpol.2019.05.008

Wei LC, Luo JX, Jiang LJ, Qiu LJ, Zhang JM, Zhang DW (2018) CoSe2 nanoparticles grown on carbon nanofibers derived from bacterial cellulose as an efficient electrocatalyst for hydrogen evolution reaction. Int J Hydrog Energy 43(45):20704–20711. https://doi.org/10.1016/j.ijhydene.2018.09.151

Xiong SL, Zhang XG, Qian YT (2009) CdS with various novel hierarchical nanostructures by nanobelts/nanowires self-assembly: controllable preparation and their optical properties. Cryst Growth Des 9(12):5259–5265. https://doi.org/10.1021/cg900780a

Yang J, Wang D, Han H, Li C (2013) Roles of cocatalysts in photocatalysis and photoelectrocatalysis. Acc Chem Res 46(8):1900–1909. https://doi.org/10.1021/ar300227e

Zeng JH, Yu Z, Liu YF, Jian Y, Qian YT, Zheng HG (2002) Morphology development of CdS/PVAc composite from spheres to rods. Mater Sci Eng B 94(2–3):131–135. https://doi.org/10.1016/S0921-5107(01)00945-X

Zhai TY, Fang XS, Bando Y, Liao Q, Xu XJ, Zeng HB (2009) Morphology-dependent stimulated emission and field emission of ordered CdS nanostructure arrays. ACS Nano 3(4):949–959. https://doi.org/10.1021/nn800895k

Zhang BX, Yu H, Zhang YB, Luo ZH, Han WJ, Qiu WF, Zhao T (2018) Bacterial cellulose derived monolithic titania aerogel consisting of 3D reticulate titania nanofibers. Cellulose 25(12):7189–7196. https://doi.org/10.1007/s10570-018-2073-z

Zhou Y, Ji Q, Masuda M, Kamiya S, Shimizu T (2006) Helical arrays of CdS nanoparticles tracing on a functionalized chiral template of glycolipid nanotubes. Chem Mater A 18(2):403–406. https://doi.org/10.1021/cm051928z

Zhou M, Chen JW, Hou CJ, Liu YJ, Xu S, Yao C, Li ZY (2019) Organic-free synthesis of porous CdS sheets with controlled windows size on bacterial cellulose for photocatalytic degradation and H2 production. Appl Surf Sci 470:908–916. https://doi.org/10.1016/j.apsusc.2018.11.207

Zhu Y, Wang Y, Zhi C, Qin L, Yang L, Liang Z (2015) Visible light induced photocatalysis on CdS quantum dots decorated TiO$_2$ nanotube arrays. Appl Catal A 498:159–166. https://doi.org/10.1016/j.apcata.2015.03.035